Canadian Conference - Pacific Conference on Earthquake Engineering 2023

Vancouver, British Columbia

June 25th – June 30th, 2023

A Review of Experimental Testing of SE-SMA Reinforced Concrete Slender Shear Walls

Dan Palermo[1*] and Austin Martins-Robalino[2]

[1]Professor, Department of Civil Engineering, York University, Toronto, ON, Canada
[2]PhD Student, Department of Civil Engineering, York University, Toronto, ON, Canada
[*] dan.palermo@lassonde.yorku.ca (Corresponding Author)

ABSTRACT

Experimental testing of slender concrete shear walls reinforced with Superelastic (SE) Shape Memory Alloy (SMA) spanning the past 15 years has provided significant lessons and knowledge of the performance of this structural system. Herein, this paper includes results from testing 4 slender walls reinforced internally within the boundary zone of the plastic hinge region with SE-SMA. The remainder of the reinforcement detailing consisted of traditional deformed steel reinforcement. Subtle differences that affected the response of the walls included the presence of starter bars at the base of the walls and the type of mechanical coupler used to connect the SE-SMA bars to steel reinforcement outside of the plastic hinge. All walls had an aspect ratio of 2.2 to promote a flexural-dominant response. In addition, no axial load was imposed on these walls to study the loading case that would result in largest transient and residual drift responses. This set considers tests conducted on the walls in their original undamaged condition as a new construction methodology. In addition, the walls were further repaired and retested, where the repair incorporated either Self-Consolidating Concrete (SCC) or Engineered Cementitious Composite (ECC) as a replacement for the heavily damaged concrete in the plastic hinge region. The incorporation of SE-SMA in the slender shear walls resulted in enhanced residual deformation control, including lateral displacements, flexural rotations, and shear straining, relative to companion steel reinforced walls. The ability to recover deformations also controlled the ratcheting of flexural rotations and shear straining in the plastic hinge region that were visible in one direction of the loading in the companion steel reinforced walls. The implementation of high-performance concreting materials, such as ECC, resulted in improved and localized damage control in the plastic hinge region.

Keywords: Shape Memory Alloys, Shear Walls, Experimental Testing, Engineering Cementitious Composite, Residual Deformations

INTRODUCTION

Four hybrid, SMA-steel slender concrete shear walls are presented in this review and were previously constructed and reported by Abdulridha [1], Zaidi [2,3], Morcos [4], and Soto-Rojas [5]. The focus is to provide a comparison of the performance of these walls based on salient performance indicators, including load-displacement responses, cracking patterns and failure modes, residual drifts, global rotation, and shear straining in the plastic hinge region. The intent is to illustrate the impact on the response due to subtle changes in the design and construction of these walls. In addition, the impact on repairing materials is also discussed.

Background

Abdulridha was the first to construct a slender shear wall which utilized SE-SMAs strategically in the plastic hinge boundary regions of the wall to maximize the recentering capabilities while minimizing cost. Lacking any codes for designing with SMA at that time, Abdulridha's approach was to first design a 3/4th scale single storey traditional steel reinforced concrete shear wall following CSA A23-3 Design of Concrete Structures. The hybrid wall followed the same procedure but substituted the deformed steel reinforcement in the boundary regions with SE-SMA bars that provided a similar tensile force. The resulting wall dimensions and reinforcement layout are shown in Figure 1. The wall had an aspect ratio of 2.2 and measured 2200 mm high, 1000 mm wide, and had a thickness of 150 mm. A foundation block measuring 500 mm high, 1700 mm wide, and 1400 mm thick allowed for the wall to be anchored to a strong floor while a cap beam measuring 400 mm high, 1700 mm wide, and 400 mm thick allowed for attachment of an actuator which applied the lateral loading. Longitudinal reinforcement consisted of two curtains of 3-10M bars spaced 150 mm apart in the web region and 2-15M bars in the boundary region above the plastic hinge spaced 120 mm apart. SE-SMAs bars present in the boundary region measured 12.7 mm in diameter and had a total length of 1200 mm extending 950 mm into the wall and 250 mm into the foundation. The SMA bars were spliced to the adjacent 15M bars using modified screw-lock mechanical couplers. Horizontal reinforcement consisted of 10M bars at 150 mm along the entire height of the wall. Additionally, 10M closed ties were present in in the boundary regions to prevent buckling of longitudinal reinforcement and spaced 75 mm apart in the plastic hinge region and 150 mm above the plastic hinge. Four, 10M starter bars, which extended from 300 mm into the foundation and 300 mm into the wall, were placed between the longitudinal reinforcement in the web to prevent sliding and rocking at the base of the wall.

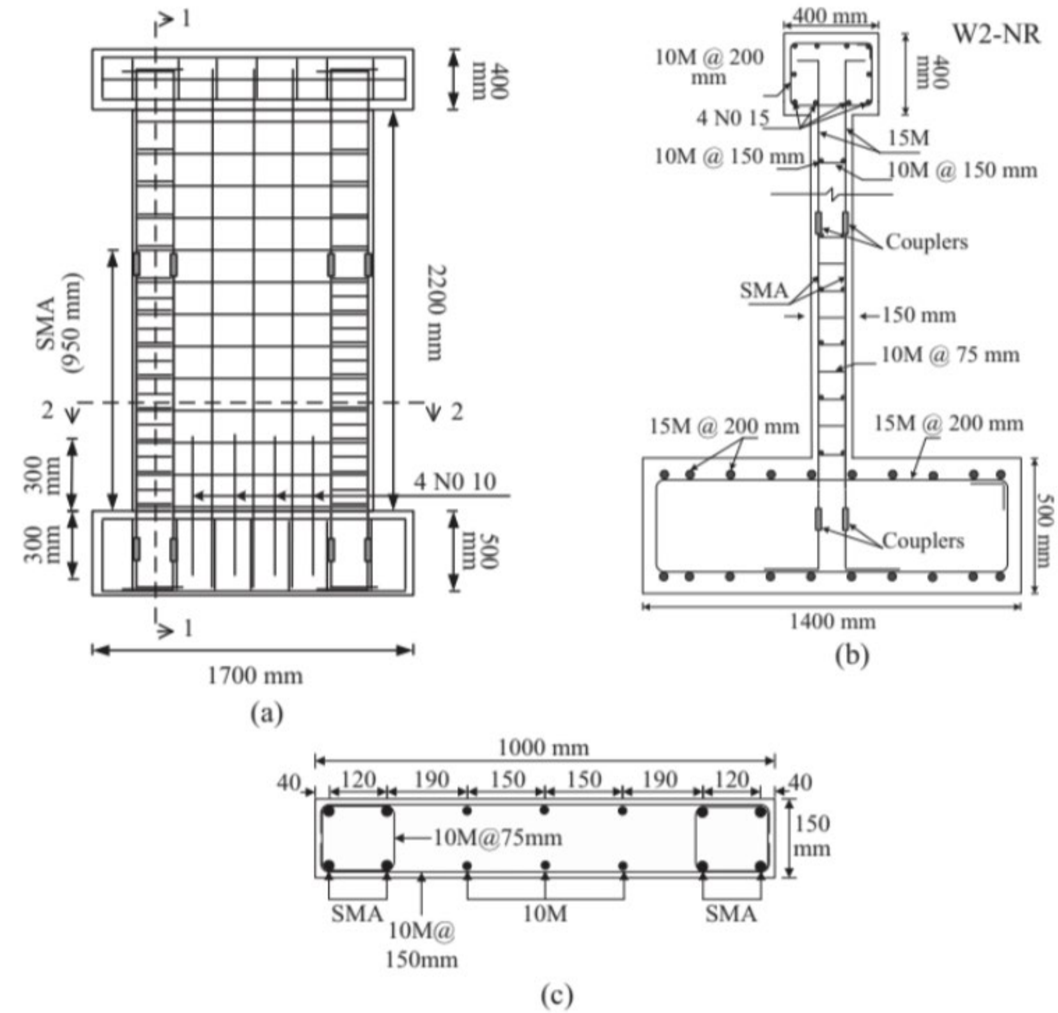

Figure 1. Reinforcement Details of Abdulridha's SMA-steel hybrid shear wall: (a) Elevation View; (b) Section 1-1; and (c) Section 2-2 [1].

The work of Zaidi examined the performance of the hybrid wall reported by Abdulridha after repair. The repairs undertaken by Zaidi included removal and replacement of heavily damaged concrete and reinforcement. Concrete was removed up to a height of 740 mm from the top of the foundation in the web region while the concrete in the boundary regions was removed up to a height of 1000 mm. This revealed multiple fractures and buckling of the steel reinforcement in the web region and moderate buckling of the SMA bars in the vicinity of a predominate crack. All starter bars were removed at the base of the wall. It was decided that the SMA bars would not be replaced but shortened from their original height of 950 mm above the base of the wall to approximately 425 mm above the base to examine the effectiveness of a reduced length. 525mm-long segments of 15M bars were used in place of the removed SMA sections while new 540 mm segments of 10M reinforcement replaced the damaged steel in the web starting at a height of 90 mm from the base. All new sections of steel were spliced to the undamaged sections of reinforcement using 4-inch screw-lock mechanical couplers. High strength Self-Consolidating Concrete (SCC) was used to replace the removed damaged concrete.

The walls constructed by Morcos followed a similar design procedure used by Abdulridha and maintained the same wall dimensions and spacing of longitudinal and horizontal reinforcement. The layout of the High Bay Lab testing facility at York University required that the width of both the foundation and cap beam be modified from the original 1700 mm to 1600 mm to allow for proper alignment of the actuator at its mid-stroke. The traditional steel reinforcement which was spliced to the SMA bars at the top of the plastic hinge was changed from 15M to #13 due to the availability of reinforcement from the manufacturer of the coupler. Additional modifications in Morcos' wall included using the same length of SMA bars but shifting their position down 50 mm to 300 mm into the foundation and extending 900 mm above the foundation, extending the 75 mm spacing ties in the boundary region to a height of 1100 mm above the wall base, and not including starter bars. The most significant modification implemented by Morcos was the use of headed reinforcement mechanical couplers (Figure 2 a)) in place of the modified screw-lock mechanical couplers used by Abdulridha and Zaidi (Figure 2 b)). The screw-lock mechanical couplers are prone to allow slip of the SMA bar before full development of its tensile properties and required modifications in the work of Abdulridha. This consisted of 18 screws to be used (compared to the 6 screws provided by the manufacturer) and the SMA bar to be inserted to the end of the coupler with the steel reinforcement welded to the end. Typically, use of these couplers require that each bar being coupled meet at the midpoint of the coupler. Examining the literature involving SMA-steel hybrid elements demonstrated a consistent need for modifications when tradition screw-lock mechanical couplers were used to splice steel and SMA [6]–[9]. Tensile testing of the headed reinforcement mechanical coupler resulted in failure of the #13 steel reinforcement before any occurrence of slip.

(a)

(b)

Figure 2. Mechanical couplers: (a) Headed reinforcement coupler [4], and (b) modified screw-lock coupler [1].

Soto-Rojas repaired the walls by Morcos after they had been tested to failure. Similar to the repair strategy implemented by Zaidi, this involved the removal and replacement of heavily damaged concrete and reinforcement in the plastic hinge. Concrete was removed starting at a depth of 60 mm into the foundation and to 1020 above the base of the wall. The 10M reinforcement in the web had fractured and buckled while there was no noticeable damage to the SMA bars. Damaged 10M reinforcement was removed from the base of the wall up to a height of 500 mm and replaced with new 500 mm length sections using 4-inch mechanical screw-lock couplers. Soto-Rojas inserted four starter bars at the same spacing and location as Abdulridha to address the significant sliding and rocking at the base of the wall observed by Morcos during testing of the walls in their original condition. Installation of these starter bars consisted of drilling 300 mm into the foundation at which point a high strength epoxy was used to bond the 600 mm long bars to the surrounding concrete. Whereas Zaidi used a commercially available SCC to replace damaged concrete, Soto-Rojas used an in house Engineered Cementitious Composite (ECC) mix, to investigate emerging materials which could provide better ductility, damage resilience, and tensile capacity compared to traditional concretes.

Herein the walls will be denoted as SWN (Shear Wall with Nitinol), followed by the initial/s of the researcher. For example, SWN-A refers to the wall reported by Abdulridha. Additionally, to provide further clarification the walls from Zaidi and Soto-Rojas have a prefix R denoting that they are repaired walls (R-SWN-Z and R-SWN-SR, respectively). The material properties for the different reinforcement and concretes in the SWN walls are presented in Table 1.

Table 1. Material Properties of Reinforcement and Concreting Materials Used in SWN Walls.

Reinforcement Properties

Reinforcement Type	Corresponding Wall	Modulus of Elasticity (GPa)	Yield Stress (MPa)	Tensile Strength (MPa)
10M	SWN-A	202	425	615
15M	SWN-A	200	440	650
SMA	SWN-A	38	380	1068
10M	R-SWN-Z	200	480	656
10M	SWN-M	186	435	564
#13	SWN-M	203	463	627
SMA	SWN-M	42	338	1034
10M	R-SWN-SR	175	430	537

Concrete Properties

Concrete Type	Corresponding Wall	Compressive Strength (MPa)
NC	SWN-A	31.6
SCC	R-SWN-Z	81.0
NC	SWN-M	39.3
ECC	R-SWN-SR	63

Loading Programs

Walls were all tested under lateral reverse cyclic loading using a displacement-controlled loading program. For Wall SWN-A, Abdulridha carried out reverse cycles based on multiples of yield displacement in line with ATC-24. This consisted of three reverse cycles at stages corresponding to $\Delta y/3$, $2\Delta y/3$, and Δy. After the yield cycle, each stage was incremented by $0.5\Delta y$, with three repetitions at each stage until $5\Delta y$ was reached at which point increments of Δy and two repetitions at each stage was imposed. The target yield displacement was predicted to be 12 mm. Zaidi used a similar methodology for Wall R-SWN-Z with two modifications: first, the increment was decreased from $\Delta y/2$ to $\Delta y/3$ for loading stages following Δy; and the experimental yield of 27 mm observed by Abdulridha during testing of SWN-A was used instead of the predicted 12 mm. The change in increment was intended to better align the displacements of Wall R-SWN-Z with the companion control shear wall. Morcos combined the ATC-24 and FEMA 461 loading protocols for the loading of Wall SWN-M. This program was developed such that the target displacements for each loading stage were based on drift ratios with the first two stages consisting of target drifts of 0.05% and 0.1% before subsequent stages were incremented by 0.1% drift until 1% drift was reached. The post 1% drift stages were incremented by 0.5% drift until 5% drift was reached. Every stage up to and including 1.5% drift consisted of 3 repetitions, while subsequent stages incorporated two repetitions. An identical loading program was utilized by Soto-Rojas for testing of Wall R-SWN-SR.

RESULTS AND DISCUSSION

Lateral Load-Displacement Responses

The lateral load-drift responses of the walls are presented in Figure 3. The displacement (drift) was captured by string potentiometers connected to the mid-height of the cap beam and secured such that the measurements were with respect to the foundation to eliminate the impact of slip and rocking between the foundation and strong floor.

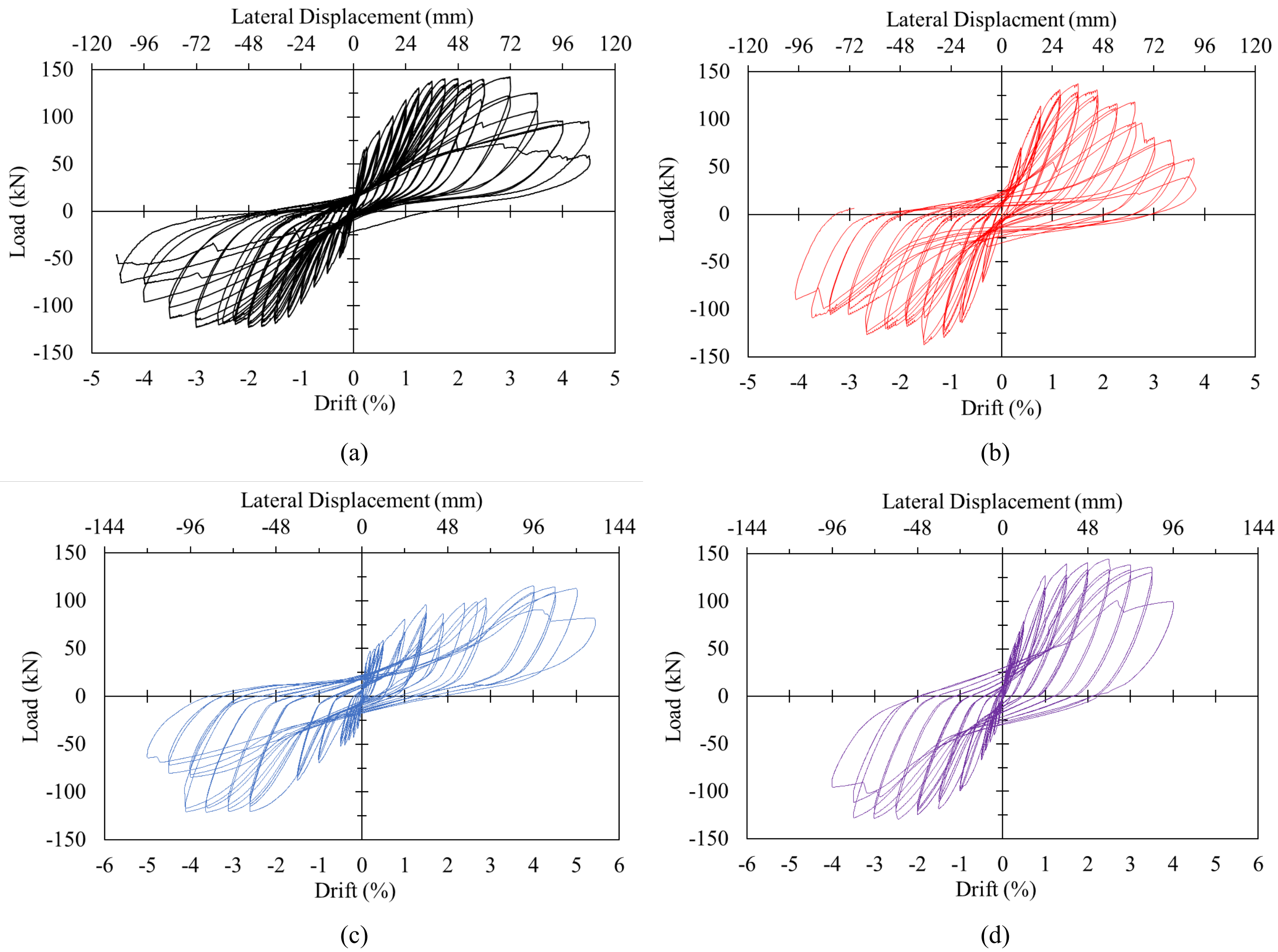

Figure 3. Lateral load-drift responses: (a) SWN-A [1], (b) R-SWN-Z [2], (c) SWN-M [5], and (d) R-SWN-SR [5].

Failure Modes

The failure of Wall SWN-A was controlled by a prominent flexural propagating through the entire length of the wall and located approximately 350 mm above the base of the wall and adjacent to the end of the starter bars (Figure 4). Failure occurred at 108 mm displacement (4.5% drift) and consisted of the wall sliding along the crack surface. Prior to failure it was noted by that concrete crushing, spalling, and buckling of an SMA bar occurred at this flexural crack. Drops in lateral load observed during the second cycle at 72 mm, the second cycle at 84 mm, and the first cycle at 94 mm correspond to rupture of longitudinal deformed steel bars in the web region adjacent to the SMA bars. Removal of damaged concrete after testing revealed that one of the SMA bars had fractured at the mechanical coupler 900 mm above the base of the wall. This SMA fracture is responsible for the last drop in lateral load which prompted the termination of the test.

Wall R-SWN-Z which lacked starter bars and had SMA bars shortened to a height of 425 mm above the base of the wall had crack formation limited to the repaired region of the wall with no new cracks forming above the plastic hinge and existing cracks only reopening. Initial cracking occurred at 140 mm, 260 mm, 440 mm, and 690 mm above the wall with the cracks at 260 mm and 400 mm corresponding to the just below and above the six-inch couplers used to connect the shortened SMA bars to the deformed steel reinforcement. Loading beyond a displacement of 54 mm (2.25% drift), it was observed that the critical crack formed at a height of 260 mm with spalling occurring in the boundaries (Figure 5). During the second 62 mm cycle (2.5% drift) an SMA bar fractured leading to drop in lateral load of 13%. Additional SMA bars fractured during the positive and negative loading of the 72 mm cycle (3.0% drift) and during the second cycle at 90 mm (3.75 % drift). All fractures were found to have occurred at the termination of couplers at approximately 260 mm above the base. The location of rupture of the SMA, directly below the location of the couplers, in both SWN-A and R-SWN-Z suggest that the screws used in the couplers induced a plane of weakness leading to premature fracture of the bars.

Figure 4. Cracking pattern of SWN-A after 72 mm (3.0% drift cycle)[1].

Figure 5. Cracking pattern of R-SWN-Z at end of testing [3].

Wall SWN-M experienced a critical flexural crack at the base of the wall that propagated the entire length (Figure 6). A second major flexural crack surfaced at 300 mm above the base along with a network of flexural-shear cracks along the height of the wall. The wall experienced sliding and rocking along the base before testing was terminated at the 120 mm (5.0% drift) displacement cycle. At this displacement cycle, longitudinal deformed steel reinforcement experienced buckling before rupturing after reloading. Removal of the damaged concrete post testing demonstrated that only the longitudinal steel reinforcement in the web region was damaged with the SMA bars showing no sign of damage at the base of the wall. Further investigation of the SMA-steel couplers 900 mm above the base of the wall also confirmed there was no damage to the SMA bars. The vertical bars in the web, adjacent to the boundary region, first ruptured at 108 mm displacement (4.5% drift).

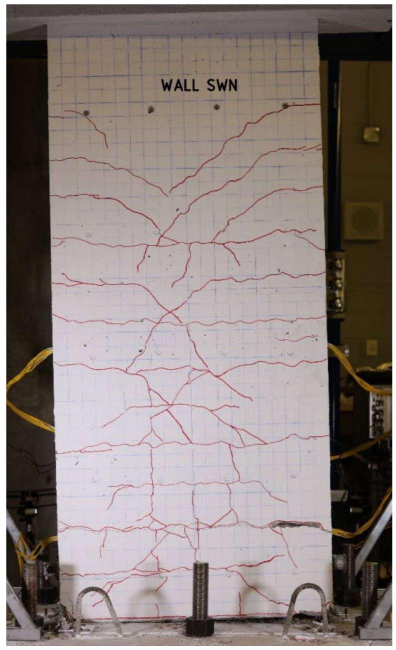

Figure 6. Cracking pattern of SWN-M after 120 mm cycle (5.0% drift) [10].

The failure plane of Wall R-SWN-SR corresponded to a crack 425 mm above the base on the left side of the wall and propagated to a crack 400 mm above the base on the right side of the wall (Figure 7). These two cracks merged in the web region of the wall at a height of 300 mm above the base, which corresponded to the location where the starter bars terminated. The first reinforcing bar rupture was experienced by a vertical steel bar in the web region adjacent to the SMA bars during the 84 mm (3.5% drift) cycle. Two additional steel bars in the web ruptured during the first 96 mm (4.0 % drift) cycle prompting the end of testing. The use of the ECC to replace damaged concrete eliminated spalling or crushing of the concrete.

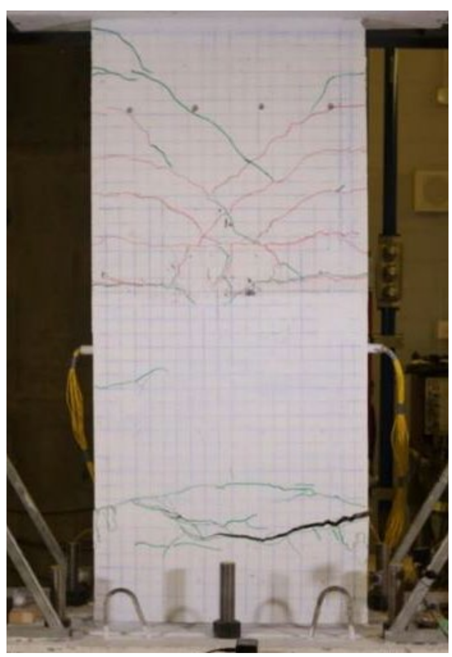

Figure 7. Cracking pattern of R-SWN-SR at end of testing [5].

The failure modes of the different SWN walls demonstrate the impact of reinforcement details and couplers. The fracture of SMA bars in SWN-A and R-SWN-Z highlight the challenges with modifications to the mechanical screw couplers. The headed reinforcement mechanical couplers used in walls SWN-M and R-SWN-SR performed significantly better; the lack of screws avoided stress localizations which lead to premature fracture in the other walls. The inclusion of starter bars in SWN-A and R-SWN-SR forced the critical crack to occur near their termination of the starter bars as opposed to the base of the wall which was in SWN-M.

Lateral Load-Drift Envelopes

The lateral load-drift envelopes of each wall are presented in Figure 8. The load and drift correspond to the first repetition at each cycle. All walls were also examined using the Park Method [11] to determine performance points, specifically the yield, peak, and ultimate of their responses which are presented in Table 2.

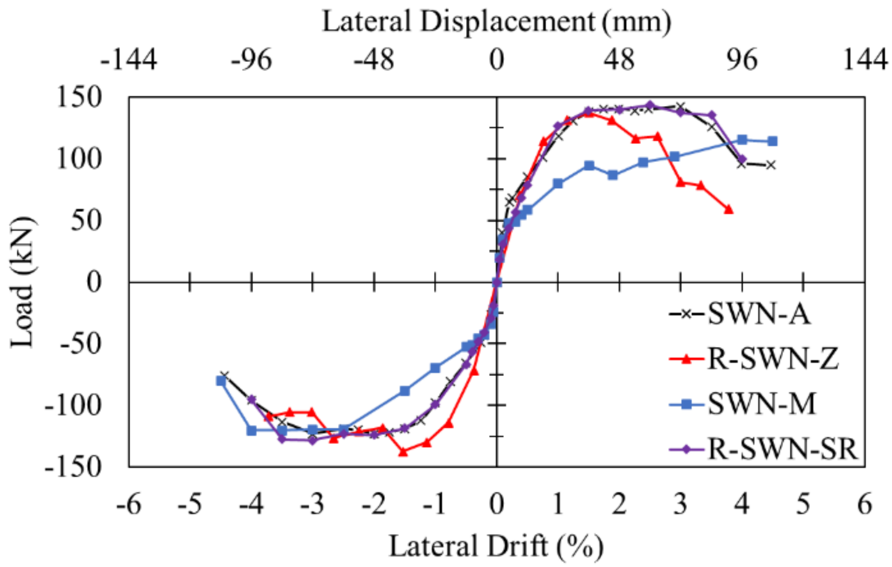

Figure 8. Lateral load-drift envelopes.

Table 2. Average Load and Displacement Performance Points.

Wall	Yield		Peak		Ultimate
	Displacement (mm)	**Load (kN)**	**Displacement (mm)**	**Load (kN)**	**Displacement (mm)**
SWN-A	26.4	112	72	133	72
R-SWN-Z	21.7	113.5	36	137.5	59
SWN-M	45	93	91	118	103
R-SWN-SR	30.9	123	59	137	84

Residual Drift

The residual drift of each wall during the first cycle is illustrated in Figure 9. The residual drift corresponded to the displacement at zero lateral load at the end of the unloading cycle for the first repetition of a given drift cycle. The residual drift at 0.5% and 2% are denoted as horizontal lines; they represent the limits for life safety and collapse prevention performance levels according to FEMA 356. Examination of these limits demonstrates that all walls were able to satisfy collapse prevention up to at least 3% peak drift. Wall SWN-A did not exceed the limit even up to peak drifts of 4.5%. Most walls satisfy the life safety performance level up to peak drifts of 1.5% in both the positive and negative loading directions with wall SWN-M only satisfying the limit up to 1% peak drift.

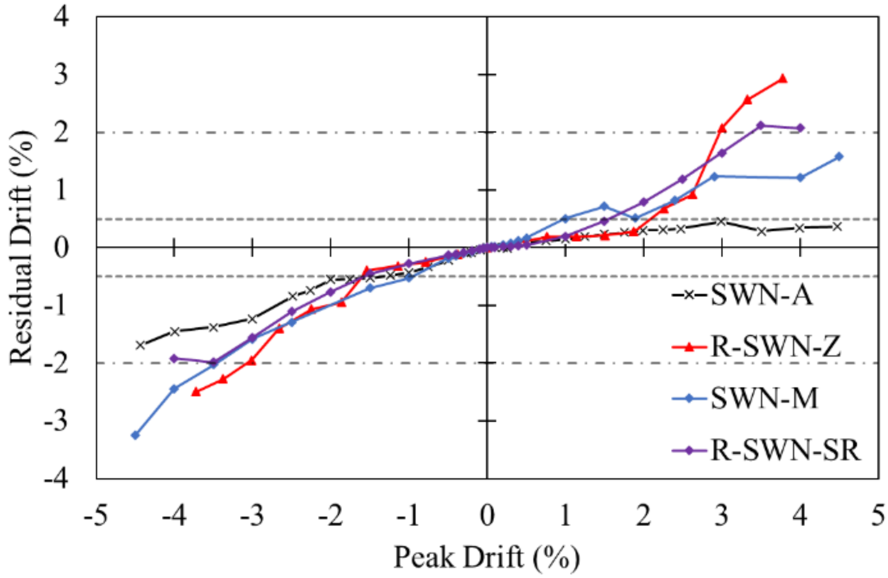

Figure 9. Residual drift-peak drift responses.

Rotation

Rotation of each wall was calculated based on two potentiometers which measured vertical displacements of the end of the cap beam with respect to the top of the foundation. The difference between these measurements divided by the distance between the instrumentation provided the rotation which are presented in Figure 10. The rotation experienced during cycles at yield, 1% drift, and 2.5% were chosen to compare the responses of the walls. Wall SWN-A had a yield drift consistent with 1% drift during which the wall experienced 11.9 x 10^{-3} rad which increased to 28 x 10^{-3} rad at 2.5% drift. Wall R-SWN-Z experienced rotations of 3.1, 6.5, and 19.4 x 10^{-3} rad at yield, 1% drift, and 2.5%, respectively. Wall SWN-M was notable for having a yield of approximately 2% drift and rotations of 24.3, 16.3, and 29.1 x 10^{-3} rad at yield, 1% drift, and 2.5%, respectively, while in Wall R-SWN-SR the rotations measured 26.9, 18.6, and 45.3 x 10^{-3} rad at yield, 1% drift, and 2.5%, respectively. The large rotations exhibited by Wall R-SWN-SR can be attributed to the lack of sliding along the critical failure crack throughout testing. In the other walls, to different extents, some of the lateral displacement recorded at the cap beam corresponded to sliding along the crack surface which would not be captured by the potentiometers used to establish the rotation of the wall relative to the base.

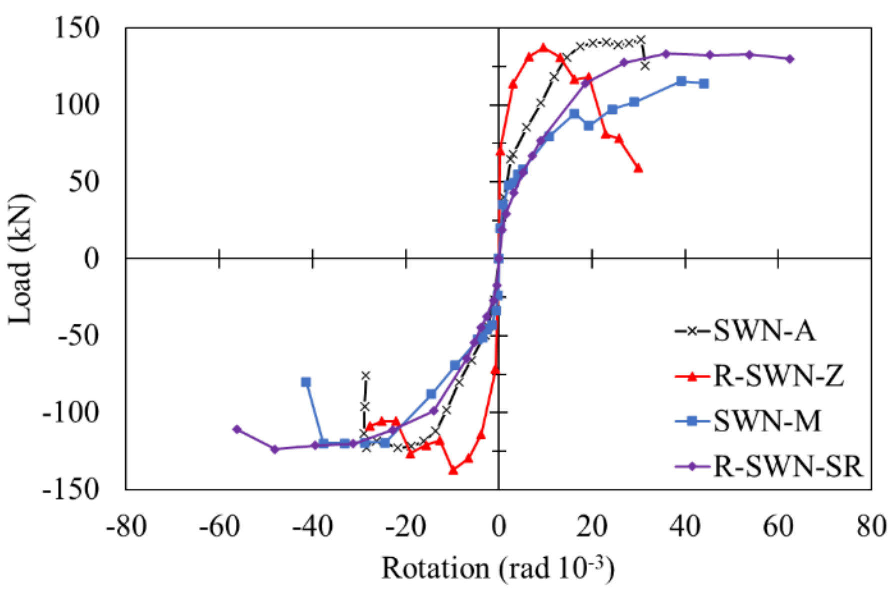

Figure 10. Lateral load-rotation envelopes.

Shear Strain

The average shear strains over the plastic hinge region of walls were calculated following Oesterle et al [12] using two string potentiometers that were placed diagonally across the wall. The lateral load-shear strain envelopes for the walls are presented in Figure 11. Note that for R-SWN-Z the full shear response is not available due to pull out of one potentiometer after the peak load was reached. Similar to the rotation responses, the shear strains experienced during cycles at yield, 1% drift, and 2.5% were chosen to compare the responses of the walls. Wall SWN-A experienced 0.29 mε which increased to 1.01 mε at 2.5% drift. Wall R-SWN-Z experienced shear strains of 0.23, 1.05, and 5.41 mε at yield, 1% drift, and 2.5%, respectively. Wall SWN-M sustained shear strains of 24.3, 16.3, and 29.1 mε at yield, 1% drift, and 2.5%, respectively; while in Wall R-SWN-SR the shear strains measured 2.78, 1.09, and 6.32 mε at yield, 1% drift, and 2.5%, respectively. The significant increase in shear strain in Wall R-SWN-SR is reflective of the greater shear capacity provided by the ECC material used in the plastic hinge and the elimination of other phenomenon such as base sliding and base rocking allowing for the response to be dominated by flexural and shear effects.

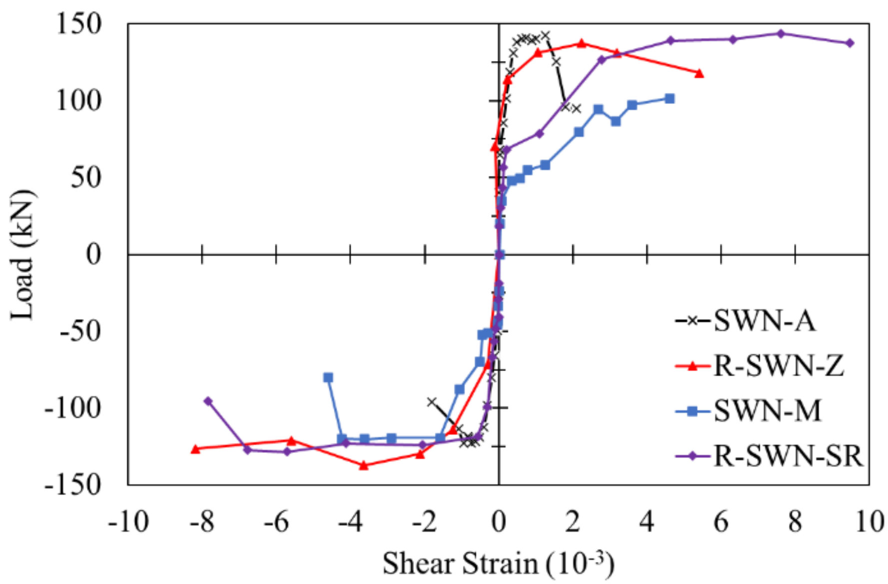

Figure 11. Lateral load-shear strain envelopes.

CONCLUSIONS

The results and performance of four, SMA-steel hybrid slender shear walls demonstrated the consistent recentering ability of SMAs. The inclusion of starter bars in these walls shifted the failure plane from the base of the wall to an area adjacent to where the bars terminated. Walls SWN-A and R-SWN-Z provided insight into the challenges faced when implementing modified mechanical couplers which can lead to premature fracture of SMA bars due to the sharp screw ends that embed into the SMA bars leading to stress localizations. Subsequent wall testing (SWN-M and R-SWN-SR) illustrated improvements provided by headed mechanical couplers, which addressed the challenges that arose in the modification of traditional screw lock couplers. Notably no damage was experienced by the SMA bars in the vacuity of the couplers even after repairing and retesting of SWN-M. Repairs provided in R-SWN-Z illustrated a simple repair method in cases where SMA bars are damaged. The use of ECC in R-SWN-SR allowed for the wall to preform similarly to wall SWM-A while sustaining significantly less damage in the form of spalling and crushing of concrete which can accelerate buckling and rupture of reinforcing bars.

REFERENCES

[1] A. Abdulridha and D. Palermo. (2017). "Behaviour and modelling of hybrid SMA-steel reinforced concrete slender shear wall," *Eng Struct*, vol. 147, doi: 10.1016/j.engstruct.2017.04.058.

[2] M. Zaidi. (2016). "Experimental Testing and Reliability Analysis of Repaired SMA and Steel Reinforced Shear Walls," Masters, University of Ottawa, Ottawa.

[3] L. Cortés-Puentes, M. Zaidi, D. Palermo, and E. Dragomirescu. (2018). "Cyclic loading testing of repaired SMA and steel reinforced concrete shear walls," *Eng Struct*, vol. 168, doi: 10.1016/j.engstruct.2018.04.044.

[4] M. Morcos and D. Palermo. (2019). "SMA-Reinforced Concrete Shear Walls Subjected to Reverse Cyclic Loading," *SMAR 2019 - Fifth Conference on Smart Monitoring, Assesment and Rehabilitation of Civil Structures*, pp. 1–8, [Online]. Available: https://www.smar2019.org/

[5] M. Soto-Rojas, A. C. Ferche, and D. Palermo. (2023). "Behaviour of Shape Memory Alloy-and Steel-Reinforced Shear Walls Repaired with Engineered Cementitious Composite," *ACI Struct J,* accepted March 2023.

[6] J. P. de Almeida, M. Steinmetz, F. Rigot, and S. de Cock. (2020). "Shape-memory NiTi alloy rebars in flexural-controlled large-scale reinforced concrete walls: Experimental investigation on self-centring and damage limitation," *Eng Struct*, vol. 220, doi: 10.1016/j.engstruct.2020.110865.

[7] M. A. Youssef, M. S. Alam, and M. Nehdi. (2008). "Experimental investigation on the seismic behavior of beam-column joints reinforced with superelastic shape memory alloys," *Journal of Earthquake Engineering*, vol. 12, no. 7, doi: 10.1080/13632460802003082.

[8] F. Oudah and R. El-Hacha. (2017). "Joint performance in concrete beam-column connections reinforced using SMA smart material," *Eng Struct*, vol. 151, doi: 10.1016/j.engstruct.2017.08.054.

[9] A. H. M. M. Billah and M. S. Alam. (2018). "Probabilistic seismic risk assessment of concrete bridge piers reinforced with different types of shape memory alloys," *Eng Struct*, vol. 162, doi: 10.1016/j.engstruct.2018.02.034.

[10] M. Morcos. (2021) "Seismic Behaviour of SMA-Reinforced Slender Concrete Shear Walls," Masters, York University, Toronto.

[11] R. Park. (1989). "Evaluation of ductility of structures and structural assemblages from laboratory testing," *Bulletin of the New Zealand Society for Earthquake Engineering*, vol. 22, no. 3, doi: 10.5459/bnzsee.22.3.155-166.

[12] R. G. Oesterle, J. D. Aristizabal-Ochoa, A. E. Fiorato, H. G. Russell, and W. G. Corley. (1979). "Earthquake Resistant Structural Walls, Tests of Isolated Walls. Phase II," *National Science Foundation, Washington, DC. Engineering and Applied Science*.